High-field electron-drift measurements and the mobility edge in hydrogenated amorphous silicon

Qing Gu and E. A. Schiff

Department of Physics, Syracuse University, Syracuse, New York 13244-1130

Jean-Baptiste Chévrier and Bernard Equer

*École Polytechnique, Laboratoire de Physique des Interfaces et des Couches Minces,
UPR 258 du CNRS, 91128 Palaiseau Cedex, France*

(Received 21 February 1995)

We report electron photocarrier time-of-flight measurements at high electric fields for two thick hydrogenated amorphous silicon (*a*-Si:H) *p-i-n* diodes. At 77 K an exponential increase in the electron mobility of more than 100 is observed as the field is increased to $E = 400$ kV/cm. The dispersion parameter was field independent. We discuss previous reports of field-dependent dispersion in terms of interface effects. We propose a model for high-field effects based on an *electric-field-dependent mobility edge* which accounts satisfactorily for the measured electric field and temperature dependence of the electron drift mobility. Effective-temperature models do not account for our measurements since they predict field-dependent dispersion. The microscopic electron mobility $\mu_0 \sim 3$ cm^2/V s is remarkably independent of electric field, temperature, and germanium alloying.

I. INTRODUCTION

For sufficiently high electrical fields, the drift velocities of charge carriers in semiconductors and insulators deviate from their linear, low-field behavior. This phenomenon is an important clue to the physics of carrier transport, which has long been exploited in crystalline semiconductors, molecularly doped polymers, and other materials.[1-4]

For amorphous semiconductors, low-field drift-mobility measurements over nearly 15 years have clearly proven the value of a phenomenological, *multiple-trapping* description of transport invoking a *transport edge* in an exponential density of states.[5-7] Carriers only contribute to transport when occupying states above this edge; carriers occupying states below the edge are trapped until thermally emitted back to the transport edge.

Perhaps surprisingly, the observation of multiple-trapping behavior has proven insufficient to discriminate between quite different fundamental mechanisms of transport; at least three distinct models have multiple-trapping behavior. The most prominent of these interprets the transport edge as a *mobility edge*:[8] an energy dividing localized from extended states. However, *hopping* of carriers between localized band-tail states also yields multiple-trapping behavior.[9-12] Still a third model invoking long-range potential fluctuations of the band edge also yields multiple-trapping behavior.[13,14]

One would hope that high-field transport effects will discriminate between these different transport models. For hydrogenated amorphous silicon (*a*-Si:H) there have now been several experiments reported.[15-25] Some of the results from the literature as well as from this work are presented in Fig. 1, where we have plotted the dependence of electron-drift velocity upon electric field for *a*-Si:H at various temperatures. The general consistency between the measurements is gratifying. For purposes of comparison we also show measurements for crystalline silicon (*c*-Si) at room temperature.

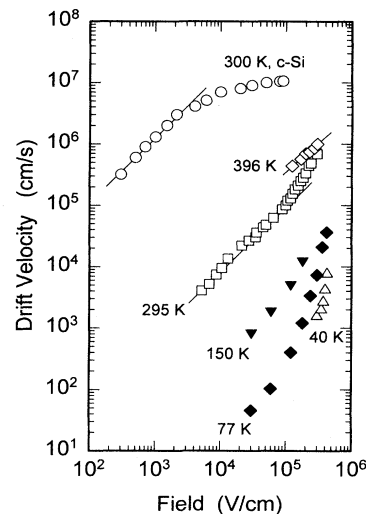We note for later reference that drift velocities in amor-

FIG. 1. Electron-drift velocity in both crystalline and amorphous silicon as the electrical field varies. The solid lines indicate low-field, linear transport. Note the superlinear transport at high fields for *a*-Si:H, and the saturated drift velocity for *c*-Si. The low-temperature values for *a*-Si:H correspond to a time 30 ns following electron photogeneration. Solid symbols are the present work on the 10-μm specimen; o, *c*-Si, 300 K (Ref. 1); ◇, 396 K (Ref. 17); □, 295 K (Ref. 18); △, 40 K (Ref. 40); ▼, 150 K (10-μm specimen); ◆, 77 K (10-μm specimen).

phous semiconductors depend strongly on the time delay between the creation of the carrier and the measurement. This "dispersive" decay is essentially a power law $v(t) \propto t^{-(1-\alpha)}$, where α is termed the *dispersion parameter*.[26,27] The great strength of the multiple-trapping description noted earlier lies in its concise description of dispersion. The data of Fig. 1 represent velocities at 30 ns after generation except as noted in the caption.

In crystalline silicon, the *saturation velocity* seen in Fig. 1, for high fields is ascribed to the emission of optical phonons by "hot" carriers with large kinetic energies. For amorphous silicon, the character of the nonlinear effect is very different, as one would expect for a material in which the effective mass theory of crystals is invalid. At 396 K (the highest temperature in Fig. 1), there is no measurable nonlinearity, although the drift velocity does approach that of c-Si. As the temperature is reduced, the velocity measured at low fields declines rapidly; this is a consequence of multiple trapping. Simultaneously the nonlinearity of the velocity with field becomes much more pronounced.

Despite the consistent pattern to these high-field measurements in a-Si:H, no consensus has emerged regarding the extensions to multiple trapping required to accommodate the high-field effects. One attractive viewpoint is that electric fields increase the *effective temperature* describing the mobility.[28,2,29–31] This viewpoint is able to accommodate the data of Fig. 1 fairly well. However, it also predicts that the the dispersion parameter α, which governs the time dependence of the drift velocity, depends markedly upon field. The field dependence is expected because the low-field dispersion parameter α is proportional to temperature, so that changes in effective temperature must show up as changes in α. The existence and character of the field-dependent dispersion effect is controversial; different research groups differ as to whether the effect exists at all in a-Si:H.

In the present work we report an extensive series of high-field photocarrier time-of-flight measurements in two thick a-Si:H p-i-n diodes especially developed as high-field detectors. The main experimental emphasis in our work has been to explore the possibility of field-dependent dispersion. The initial work from our laboratory found no evidence of this effect,[19] but this work used a fairly limited range of electric fields. Later work, in some cases using significantly larger fields, reported observation of the field-dependent dispersion.

In Sec. III, we present measurements that show that photocarrier absorption in the p^+ layer can lead to field-dependent effects, which are similar to those expected from field-dependent dispersion. Since the conventional procedure for time-of-flight uses illumination absorbed near the top interfaces of a sample, these effects can have a significant influence on measurements. We present a procedure for diagnosing these artifacts, and show that careful choice of the illumination wavelength in the photocurrent measurements can evade them. We present our measurements of the electron-drift mobility in a-Si:H in Secs. IV and V. Some of the measurements are presented in Fig. 2.

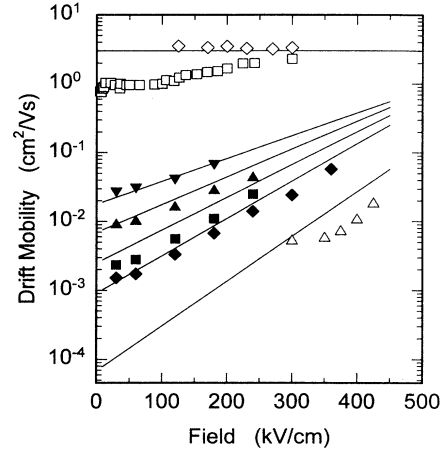We found no clear evidence for field-dependent dis-

FIG. 2. Field dependence of electron-drift mobility at specified temperatures. For temperatures below 200 K, the mobility is the transient value measured at 30 ns following electron photogeneration. The solid symbols are the present work on the 10-μm specimen. The solid lines are a fitting based upon extension of multiple trapping to incorporate an electric-field-dependent attempt frequency $\nu = \nu_0 \exp(-E/E_0)$; the parameters are $\nu_0 = 8.7 \times 10^{11}$ Hz, $\mu_0 = 3$ cm^2/Vs, $\mathcal{E}_0 = 23$ meV, and $E_0 = 57$ kV/cm. $\diamond$, 396 K (Ref. 17); $\square$, 295 K (Ref. 18); $\triangle$, 40 K (Ref. 40); $\blacktriangledown$, 150 K; $\blacktriangle$, 125 K; $\blacksquare$, 100 K; $\blacklozenge$, 77 K.

persion in the present work. We presume that the experimental difficulties just described are the root of the controversy regarding field-dependent dispersion in a-Si:H; we discuss previous work from this perspective in Sec. VII. We present a simple procedure for assessing effective-temperature descriptions of the high-field effects in Sec. VI, and show that these give a poor description of our measurements. This poor fit is quite interesting, because two independent calculations[29,30] indicate that the field dependence of transport within the band-tail hopping model has effective-temperature behavior.

We successfully fitted most measurements by invoking an electric-field-dependent attempt-to-escape frequency $\nu(E) = \nu_0 \exp(-E/E_0)$ for the band tails in the multiple-trapping model. In Fig. 2, we have superposed these fits to the field-dependent drift-mobility measurements from several laboratories ranging from 40 to 396 K. We accommodate the field dependence over the entire range of temperatures by adding a single new parameter to multiple trapping. The details of this fitting are shown in Sec. VI, where we also show that this fitting accounts for the dispersion properties of our measurements.

We believe that a field-dependent attempt frequency is a plausible consequence of a field-induced motion of the mobility-edge $\mathcal{E}_c$ in a-Si:H. A field-dependent "attempt-to-hop" frequency has previously been suggested in polymers.[32] In the absence of an electric field, the localization length is expected to diverge for band-tail states just below the mobility edge; an electric field would greatly modify such states, leading to delocalization for sufficiently shallow states. We have illustrated this idea in Fig. 3; the change in the density of states at
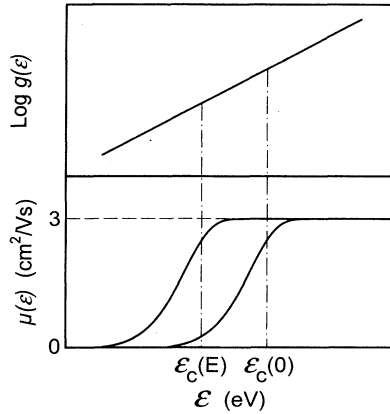
FIG. 3. Schematic diagram of the shifting of the mobility edge upon electric field as indicated by vertical dashed lines (top). The bottom part shows the resulting change on mobility due to this shift. The horizontal dashed line shows the satuated mobility value of 3 cm^2/Vs as measured by Devlen et al. (Ref. 17).

$\mathcal{E}_c$ as it moves requires a related change in the attempt frequency. We discuss these ideas in somewhat greater detail in Sec. VIII.

Perhaps the most interesting implication of the present view is not that the field moves a mobility edge, but rather that our fitting suggests that this motion does not affect the fundamental mobility parameter μ_0. μ_0 is also nearly independent of the large changes in conduction band-tail states induced by germanium alloying. We therefore speculate that μ_0 is at least to some degree a universal attribute of mobility edges.

II. SPECIMENS AND INSTRUMENTATION

The specimens were prepared at Ecole Polytechnique, Palaiseau as part of a project to develop radiation detectors. In this project it was discovered that the maximum field sustainable in a detector could be enhanced by using a fairly thick p^+ layer.[33] This aspect of the specimens plays a significant role in the present study because it fortuitously revealed an unexpected effect in the drift-mobility measurements, which was traced to optical absorption in the p^+ layer. The two structures we studied are summarized in Table I; the p^+ layers were prepared

using trimethylboron/silane mixtures (0.55% gas phase ratio). Note that the deposition sequence differs for the two specimens.

Drift mobilities were measured with a conventional photocarrier time-of-flight setup, which is described elsewhere.[24] In these measurements the bias voltage is applied across the diode about 800 μs before the laser pulse arrives; we built a special high-voltage switch for this purpose. The laser illumination pulse for this apparatus is 3 ns long; the fundamental bandwidth of the recording electronics is 125 MHz, although in practice this was usually reduced to 20 MHz. Photocurrent measurements were done by recording the voltage generated across a 50-Ω resistor (for the range 0–10^4 ns) or across larger resistors for longer times. We measured photocharge by directly recording the voltage across an RC network chosen to have a time constant longer than the maximum recording time, which was typically 100 μs.

III. TRANSIENT PHOTOCURRENT MEASUREMENTS: WAVELENGTH DEPENDENCE

The standard procedure for time-of-flight experiments uses strongly surface-absorbed light to create a thin sheet of photocarriers near the top or bottom of a film. The wavelength usually used for a-Si:H material is typically 500 nm, for which the absorption length $1/\alpha$ is 1000 Å. As the photocarriers drift across the sample, they induce a current that lasts until they are collected.

In measurements with p-i-n diodes, this conventional procedure needs to be considered carefully. To study electron motion one wishes to illuminate the specimen through its p^+ layer; an external reverse bias voltage then forces electrons to drift across the sample to its n^+ layer. The high-field diodes studied here utilize quite thick p^+ layers, which can absorb a significant fraction of the incident light. The photocarriers generated in these p^+ layers may cause difficulties in applying a conventional time-of-flight analysis, which assumes a homogeneous film.

We explored this possibility by studying the wavelength dependence of the transient photocurrent at fairly low fields. For our shortest wavelength, essentially all the light was absorbed in the p^+ layer; for our longest wavelength, only a few percent of the light was absorbed there. We found that measurements conducted when any significant fraction of the light is absorbed in the p^+ layer

TABLE I. Characteristics of the samples. CTO indicates a conductive, transparent oxide coating on the glass. d is the thickness of the intrinsic layer; d_{p+} is the thickness of the p^+ layer; d_{n+} is the thickness of the n^+ layer; C is the sample capacitance; μ_e is the average electron-drift mobilities at 150 K evaluated at $L/E = 2 \times 10^{-9}$ cm^2/V; Code is the deposition laboratory serial number.

Structure	d (μm)	d_{p+} (μm)	d_{n+} (μm)	C (pF)	μ_e (cm^2/Vs)	Code
glass/CTO/n/i/p/Al	5.0	0.17	0.06	60	6.0×10^{-3}	203 161
glass/CTO/p/i/n/Cr	10.0	0.12	0.06	30	1.7×10^{-2}	309 271

yield anomalous transients. This fact may be of importance to the interpretation of previously published high-field drift-mobility measurements.

In the present work we studied high-field drift effects using fairly weakly absorbed illumination ($\lambda \sim 700$ nm). While it is clear that the artifacts associated with light absorbed in the p^+ layer must be carefully avoided in drift-mobility studies, we were able to use the short-wavelength transients to estimate the absorption length for light in the p^+ layer and a mobility-lifetime product for electrons in the p^+ layer. The latter estimate is of some interest in its own right.

A. Measurements

We measured transient photocurrents using three laser wavelengths: 510 nm, 640 nm, and 700 nm. We can roughly estimate the percentage of the light that is absorbed in the p^+ layer from the published data on the absorption of comparable boron-doped a-Si:H.[34,35] At 510 nm, the absorption length is about 1000 Å; 70% of the light is absorbed in the p^+ layer. At 640 nm, the absorption length is about 1 μm; ($\sim 15\%$) of the light is absorbed in the p^+ layer. Finally, at 700 nm the absorption length is about 3.2 μm, and roughly 4% of total carriers are absorbed in the p^+.

In Fig. 4, we present transient photocurrent families $i(t)d^2/Q_0 V$ for these three wavelengths at 150 K. d is the specimen thickness. Each family is generated by using different pulsed bias voltages V; the resulting fields $E = V/d$ are indicated for each transient. Finally, we estimated the total photocharge Q_0 generated in the specimen by integrating the photocurrent to 40 μs using a very large collection field of 3×10^5 V/cm.

Of the three families, only the one generated at 700 nm has the classic form required for a straightforward, electron time-of-flight interpretation.

(1) Each transient shows two power-law segments, "pretransit" and "post-transit." The time separating the two segments is a characteristic transit time t_T.

(2) The pretransit segments depend linearly on the applied voltage, so the normalized currents $i(t)d^2/Q_0 V$ superpose.

The anomalous behavior of the 510 and 640 nm families is *not* a consequence of nonlinearity, and will be analyzed in the next section.

In Fig. 5 we have plotted the electric-field dependence of the photocharge $Q(E)/Q_0$ collected by $t_c = 40$ μs after the illumination pulse; $Q(E)$ is the integral of the photocurrent $i(t)$. For all three wavelengths there is a high-field plateau, which corresponds to complete collection of the photogenerated carriers; as noted earlier, we used the values of $Q(E)$ at 300 kV/cm to estimate Q_0 for each wavelength.

For the 700-nm curve, the plateau in Fig. 5 is reached at fairly low fields; fractional collection $Q(E)/Q_0 \sim 0.5$ is reached at $E \sim 10$ kV/cm. This behavior is consistent with Fig. 4, where for 700 nm the transit time t_T becomes shorter than the collection time $t_c = 40$ μs at about this field. For illumination at 510 and 640 nm, substantially
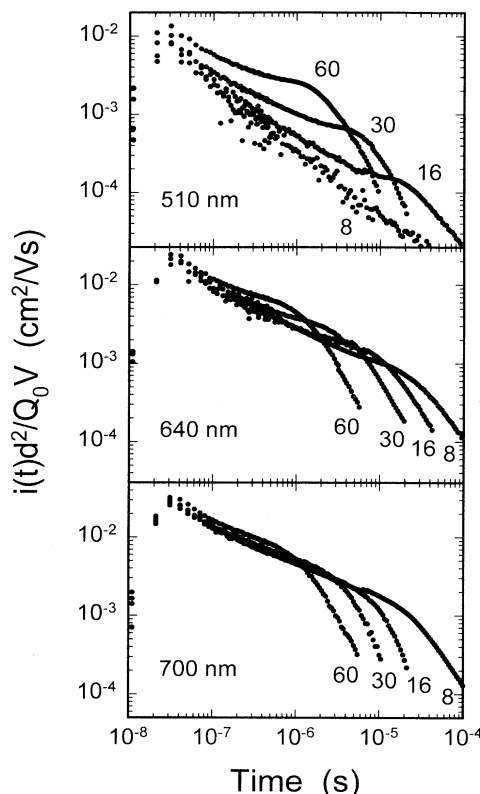

FIG. 4. Effects of illumination wavelength upon transient photocurrent measurements at 150 K (10-μm sample); the specimen was illuminated through its p^+ layer. The three panels show the normalized transient photocurrent $i(t)d^2/Q_0 V$ at 510 nm, 640 nm, and 700 nm. Each curve within a panel corresponds to a different applied field (indicated in kV/cm). Only the 700-nm transients have the form required for a straightforward time-of-flight interpretation.
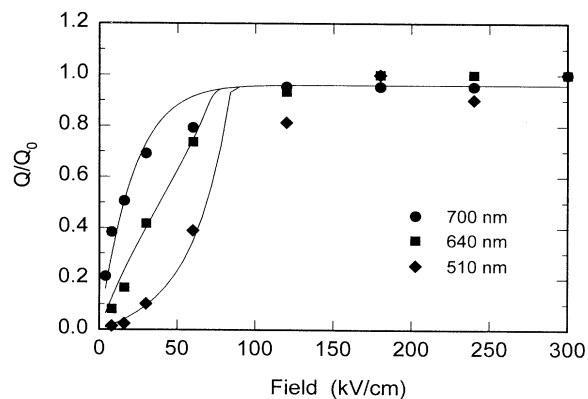

FIG. 5. Normalized photocharge $Q(E)/Q_0$ at 40 μs corresponding to the transients of Fig. 4. The 700-nm curve is fitted using the standard Hecht procedure. The 510-nm and 640-nm curves are fitted using the p^+ bleeding model described in the text.

larger fields were required to achieve charge collection of 0.5; we present an analysis of this effect in the next section.

B. Model for p^+ bleeding

In this section we describe a model for the anomalous transients measured when there is substantial absorption of light in a p^+ layer. In essence, we assume that electrons photogenerated inside the p^+ layer can be drifted into the intrinsic layer by the external field; we call this p^+ bleeding. In particular, electrons generated within a distance $\mu\tau_{e,p}E$ of the p^+/i interface will reach the intrinsic layer and hence contribute to the collected charge $Q(E)$; $\mu\tau_{e,p}$ is the electron (i.e., minority carrier) mobility-lifetime product in the p^+ layer.

We first review the "Hecht" form expected for $Q(E)/Q_0$ in the absence of this bleeding effect, which is the usual situation for time-of-flight measurements:

$$Q(E)/Q_0 = 1 - \exp(-\xi_i E/d_i) , \qquad (1)$$

where d_i is the thickness of the intrinsic layer and $\xi_i E$ is the mean drift or displacement of electrons in intrinsic material during the collection time t_c.

In order to treat the p^+ layer one needs to know whether the pulsed bias voltage used in these low-temperature experiments creates a uniform electric field in both the p^+ as well as the intrinsic layer. At 150 K, the conductivity of the p^+ layer is about $\sigma_p \sim 10^{-12} \ \Omega^{-1} \text{cm}^{-1}$; the corresponding dielectric relaxation time $\tau_d = \epsilon\epsilon_0/\sigma_p \sim 10^2$ s much larger than the bias voltage pulse width of about 10 ms.[36] For simplicity we assumed that the fields in the p^+ and the intrinsic layers were the same—neglecting any small differences in their dielectric constants.

The distribution of photocarriers inside the p^+ layer is proportional to $\exp(-\alpha_p x)$, where α_p is the absorption coefficient in the p^+ layer at the laser wavelength. A short calculation reveals that the fraction $f_c(E)$ of photogenerated carriers that are generated either in the intrinsic layer or in the p^+ layer, but within $\mu\tau_{e,p}E$ of the p^+/i interface, is

$$f_c(E) = \exp(-\alpha_p[d_p - \mu\tau_{e,p}E]) , \qquad (2)$$

where d_p is the thickness of the p^+ layer.

Combining the possibility of p^+ bleeding [Eq. (2)] with the standard partial collection result [Eq. (1)] yields

$$Q(E)/Q_0 = [1 - \exp(\xi_i E/d_i)] \exp(-\alpha_p[d_p - \mu\tau_{e,p}E]) . \qquad (3)$$

We applied this model to the 510 nm and 640 nm $Q(E)/Q_0$ data in Fig. 5. We used the 700-nm data to estimate $[1 - \exp(\xi_i E/d_i)]$ since almost all the photogenerated carriers were in the intrinsic layer. The fitting parameters that emerged were 510 nm, $\alpha_p = 2.5 \times 10^5$ cm^{-1}, $\mu\tau_{e,p} = 1.2 \times 10^{-10}$ cm^2/V; 640 nm, $\alpha_p = 8 \times 10^4$ cm^{-1}, $\mu\tau_{e,p} = 1.4 \times 10^{-10}$ cm^2/V.

C. Discussion

As noted previously, the 700-nm transients can be interpreted without consideration of the p^+ layer effects. The p^+ bleeding model just described appears to give a satisfactory qualitative description for the anomalous charge collection for the 510-nm and 640-nm transients. The $\mu\tau_{e,p}$ products estimated from the two wavelengths agree well. The absorption coefficient α_p fitted at 510 nm is in good agreement with the literature; the value fitted at 640 nm is too large, which may indicate a breakdown in the model.

Mobility-lifetime products exactly comparable to the ones we have estimated have not been previously reported. However, Street, Zesch, and Thompson[37] reported electron deep-trapping mobility-lifetime products in B-doped a-Si:H; they found that $\mu\tau_{e,p}$ had already declined to 10^{-10} cm^2/V with a doping level of 10^{-4}, which is somewhat lower than used here.

It is useful to reexamine the transients for 510 nm and 640 nm in the light of this bleeding model. Roughly speaking, the higher-field transients yield comparable "apparent" transit times for all cases, so drift-mobility estimates based on transit times are probably not grossly affected by p^+ absorption. On the other hand, if one wishes to estimate a dispersion or other parameter based upon the exact form of the transient, it is clear than there can be no substantial absorption in the p^+.

IV. LOW-FIELD MEASUREMENTS

In this section we present our measurements and estimates of the electron-drift mobility as a function of temperature; only measurements done in the linear, low-field domain are presented. These data establish that the present measurements are comparable to prior work.

For the reasons described in the last section, we needed to use 700-nm illumination for measurements in the 10-μm sample. The 5-μm sample was also studied using this wavelength, but for this specimen illumination was through the n^+ layer. This illumination wavelength is very weakly absorbed in undoped, intrinsic a-Si:H layers[34,35] ($\alpha_i \sim 3 \times 10^3$ cm^{-1}). We shall treat it as uniformly absorbed in the intrinsic layer, which is an adequate approximation when $1/\alpha_i \sim d/2$, where d is the thickness of the intrinsic layer.

A. Photocharge collection

In Fig. 6 we have plotted the photocharge at 40 μs as a function of applied external fields for the 10-μm specimen for several temperatures. Measurements on the 5-μm specimen yielded similar results, which we shall not present here.

The essential feature is that a saturated value is reached for all temperatures for sufficiently large electric fields. At 298 K, this saturation corresponds to collection of both electrons and holes from the structure within the
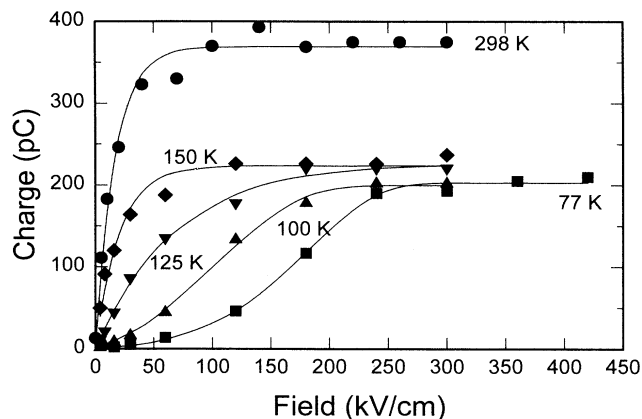
FIG. 6. Photocharge measurements as a function of applied field for the temperature range 77 K $\sim$ 298 K (10-μm sample). The solid lines are fits using an exponential dependence of the mobility on field.

FIG. 7. Low-field mobility measurement in 5-μm sample using 700 nm. The numbers under each curve are the corresponding fields in kV/cm. The results show a good low-field linear transport. Conduction band-tail width estimated from dispersion parameter is about 24 meV. Also shown in this graph is the fast shrinking transit time with increasing field, which causes loss of time resolution at high fields.

40-μs collection time. Prior work on holes shows that the ratio L_h/E of the hole displacement L_h and the electric field E is 3×10^{-8} cm^2/V at 40 μs and 298 K. Hole collection will be apparent when $L > d/4$ (for a uniform distribution of holes), or for $E > 10^4$ V/cm. This estimate is in good agreement with the figure.

At lower temperatures the saturated charge is about half that at 298 K. The halving is a consequence of the fact that hole collection within 40 μs is negligible at 150 K and below; the collected charge is due only to electrons. Correspondingly, we shall neglect the contribution of hole motion to the transient photocurrents at 150 K and below, and indeed we implicitly did this in the last section.

At 150 K the Q versus E plot has the simple Hecht form: a linear rise for lower fields that saturates for high fields. The slope of the low-field portion can be used to extract the displacement/field ratio L/E for electrons at 150 K and 40 μs. For simplicity, we denote L/E as the electron displacibility $\xi(t_c)$. For uniform illumination, we use the approximation

$$Q(E) = (Q_0/2) \{1 - \exp[-2\xi(t_c)E/d]\} . \qquad (4)$$

A somewhat more exact treatment was given by Antoniadis and Schiff.[38] The form is basically a consequence of assuming that the displacement (or *Schubweg*) L depends linearly on electric field.

The curves at temperatures below 100 K lose the Hecht form, adopting a sort of "S" shape. This is in fact clear evidence for a breakdown in the assumption of linearity, which is the central subject of this paper. As will be developed more fully later in the paper, these nonlinear effects increase all displacements exponentially:

$$\xi(t_c, E) = \xi(t_c) \exp(E/E_1) . \qquad (5)$$

The solid lines in Fig. 6 are the fits using this exponential form and the values for E_1 reported in the next section.

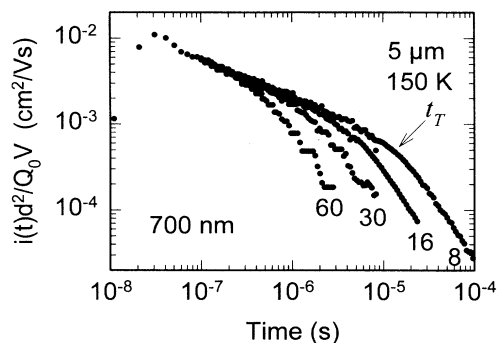We note in conclusion that some early work on field-

dependent effects invoked field-dependent photogeneration quantum efficiencies. At present we have no evidence at all in drift-mobility studies for any such field dependence; a more complete discussion of this issue has been given previously.[39,19,40]

B. Average drift mobilities

In Fig. 7, we have plotted normalized photocurrents transients $i(t)d^2/Q_0V$ at several bias fields for the 5-μm sample at 150 K.

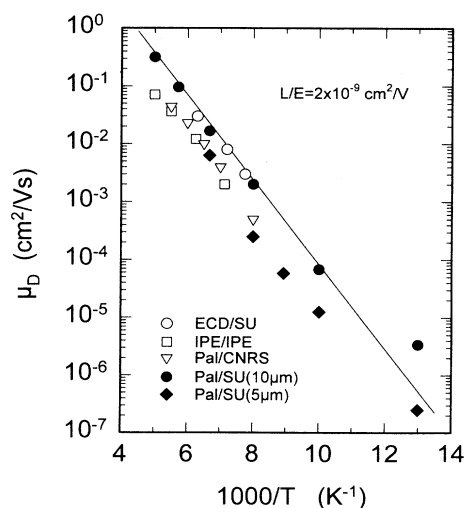In Fig. 8, we have compared electron-drift mobility

FIG. 8. Average electron-drift mobility μ_D as a function of reciprocal temperature in undoped a-Si:H from several sources. μ_D was evaluated in all cases for a displacement field ratio $L/E \sim 2 \times 10^{-9}$ cm^2/V; the procedure is discussed in Ref. 41. Solid symbols are this work; open symbols indicate previous reports. The solid line is a fit to 10-μm data using the same set of parameters as shown in Fig. 2.

estimates as a function of temperature from five differ-ent sources; the detailed references are given in the figure caption. It is clear that all of these differing specimens give similar results; we believe that the modest differ-ences apparent in Fig. 8 are statistically significant.

We note that this type of comparison is only valid if the drift mobilities are compared for a constant ratio of elec-tron displacement L and electric field E. For example, if the estimates are obtained from conventional transit time estimates, then $\mu_D = L/Et_T = (d/2)/Et_T$. To compare specimens with different thicknesses d, one must use elec-tric fields that are changed so as to keep the ratio d/E constant. This procedure was first introduced by Wang, et al.,[41] where an exhaustive discussion may be found. In most work from our laboratory, we have chosen to com-pare differing materials using $L/E \sim 2 \times 10^{-9}$ cm^2/V, which is small enough to avoid deep-trapping effects in most cases.

V. HIGH-FIELD MEASUREMENTS

The simplest procedure for discerning genuine non-linear transport in a-Si:H is simply to examine the de-pendence of the transient photocurrent $i(t)$ upon the electric field E at a time sufficiently early that car-rier transit is unimportant. In the transients at 150 K (Fig. 4) measured at 700 nm, one sees that the nor-malized transients $i(t)/V$ measured at fields in the range 8–60 kV/cm have the same magnitude in their pretransit regime, as expected for linear, Ohmic transport. In the post-transit region, the normalized transients $i(t)/V$ de-crease strongly with field, but this behavior is due simply to carrier sweepout effects.

In Fig. 9, we present transient photocurrents in the 5-μm p-i-n structure at 77 K using 700-nm illumination. Here we have shown transients for fields sufficiently large
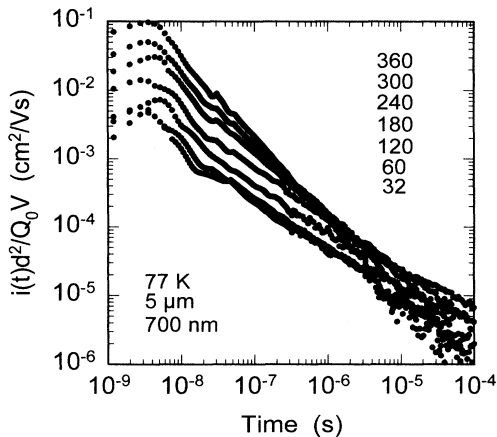

FIG. 9. Normalized transient photocurrents in 5-μm sam-ple measured at 77 K. The early time sections of the tran-sients were treated by using the Fourier transform method described in Ref. 24. The later time sections were measured directly. The corresponding applied fields for the transients are listed in the figure in kV/cm.
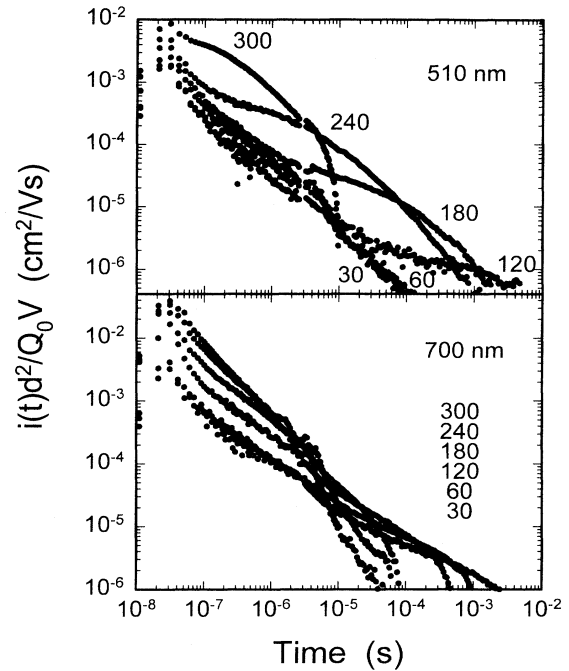

FIG. 10. Effects of illumination wavelength on normalized transient photocurrents $i(t)d^2/Q_0V$ measured at 77 K (10-μm sample). The applied field $E = V/d$ is indicated for each curve. The qualitative difference between the two sets of tran-sients is attributed to photogeneration in the p^+ layer at 510 nm; the 700-nm measurements were used to study electron drift.

that linearity has clearly broken down. The early time behavior of the transients is strongly superlinear in field E; at 30 ns, $i(t)$ has increased nearly 30 times faster with field in the range 30–360 kV/cm than predicted by linear transport.

In Fig. 10 we present transient photocurrents for the 10-μm p-i-n structure at 77 K using both 700-nm and 510-nm illumination. As discussed previously, only the 700-nm illumination gives acceptable low-field behavior. As for the 5-μm specimen, one observes a strongly super-linear increase of $i(t)$ with field E at the earliest times. It is also clear that there is a very substantial difference in transients measured at the two illumination wavelengths, which reemphasizes the importance of avoiding substan-tial absorption in the doped layers of the structure.

We find it easier to grasp the nonlinear transport im-plications of transients such as those in Fig. 10 by plot-ting the normalized photocurrent $i(t)d^2/Q_0V$ at particu-lar times in the transient as a function of field. We have done this in Fig. 11 for the data of Fig. 10; we have also included data from additional transients at still higher fields, which were left out of Fig. 10 to reduce its clutter. The smooth curves are our fits to these data, which will be described in the next section.

In brief, the dependence of $i(t)d^2/Q_0V$ upon field $E = V/d$ shows two regimes. At lower fields there is an essentially exponential rise. This rise terminates for fields sufficiently large that carrier sweepout occurs be-
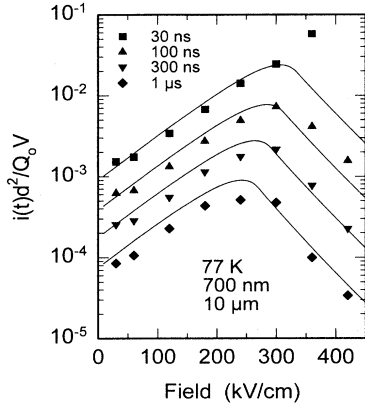
FIG. 11. Semilogarithmic graph of the transient photocurrent $i(t)d^2/Q_0V$ as a function of field $E = V/d$ at 77 K in 10-μm sample. The results are given for four different delay times t as noted in the figure. The solid curves are fits based on the field-dependent attempt frequency $\nu = \nu_0 \exp(-E/E_0)$ and band-tail multiple trapping. The parameters are the same as shown in Fig. 2.

fore t, and there is a rollover to an exponential decline in $i(t)d^2/Q_0V$ for larger fields. When shorter times are used, the rollover between the two regimes of field dependence occurs for larger fields, which is consistent with the idea that the rollover reflects the onset of carrier sweepout. The magnitudes of $i(t)d^2/Q_0V$ are largest for earliest times, which is just a consequence of the power-law transient decay of $i(t)$.

For the 30-ns data, we don't see the rollover effect; we believe that this is a consequence of the electrical response time in these measurements, which was about 12-ns. The transient current decays in time essentially as $t^{-0.75}$; the singular behavior near $t = 0$ causes the effects of the 12-ns response to persist for surprisingly long times in the transient. For the data in Fig. 9, we achieved a much reduced response time using a rather time consuming procedure,[24] which was not used for Fig. 10.

VI. MODELS FOR HIGH-FIELD TRANSPORT

A. Low-field transport

We start by reviewing the predictions of the exponential band tail, multiple-trapping model.[42] This model is the simplest one that accounts adequately for temperature-dependent photocarrier drift measurements in the low electric field, linear limit. For an exponential band tail with a decay parameter $\mathcal{E}_0$, one can derive a transient drift mobility to describe linear transport:

$$\mu(t) = 2\mu_0\alpha(1 - \alpha)(\nu t)^{-(1-\alpha)}. \tag{6}$$

Here ν is the common band tail trap attempt-to-escape frequency, $\alpha = k_B T/\mathcal{E}_0$ is the temperature-dependent

dispersion parameter, and μ_0 is a "microscopic" mobility characterizing the transport channel. As noted in the Introduction, at least three microscopic mechanisms have been identified that yield this multiple-trapping form.

Once the form of $\mu(t)$ is known, one can predict the normalized photocurrent transients $i(t)d^2/Q_0V$, both before and after the characteristic photocarrier transit time t_T across the specimen thickness d (we are assuming that photocarriers traverse the entire sample).[43] For the present case of band-tail multiple trapping,

$$i(t)d^2/Q_0V = \mu(t) \quad (t < t_T), \tag{7}$$

$$i(t)d^2/Q_0V = 2\mu_0\alpha(1 - \alpha)$$
$$\times (\nu t_T)^{2\alpha}(\nu t)^{-(1+\alpha)} \quad (t \geq t_T), \tag{8}$$

$$t_T = \left(\frac{1}{\nu}\right)\left(\frac{\nu d}{(1 - \alpha)\mu_0 E}\right)^{\frac{1}{\alpha}}. \tag{9}$$

For the 10-μm specimen, we obtained an adequate agreement with our measurements using the same parameters shown in Fig. 2; the resulting fitting to the average mobility is indicated by the solid line in Fig. 8.

B. Extension to high fields: General remarks

The low-field, exponential band-tail model of Eq. (6) suggests three possibilities for generalization to high fields: (1) The microscopic mobility μ_0, (2) the dispersion parameter, and (3) the attempt-to-escape frequency ν.

The first possibility, that μ_0 might increase with field, is certainly sensible. Analogous effects are known in crystals, and in amorphous semiconductors the existence of polarization-dependent electroabsorption indicates that electric fields do modify the character of wavefunctions near the transport edge.[44,45] However, we believe the field dependence of μ_0 is unsatisfactory as a model for the high-field effects. Devlen, Tauc, and Schiff[17] found that there is little field dependence to the electron mobility at temperatures $T > 396$ K (cf. Fig. 2); even near 300 K, the field dependence is modest. These measurement suggest that field dependence is associated with the trapping and detrapping mechanisms in the low-field model. The strong temperature dependence to the electron-drift mobility for $T < 300$ K is certainly associated with these processes. A strong field dependence is only observed in this same low-temperature regime.

The second possibility is that an electric field modifies the dispersion parameter α. Since for multiple trapping the dispersion parameter is essentially proportional to temperature $\alpha = k_B T/\mathcal{E}_0$, this idea is equivalent to saying that high-fields effects can be described using an *effective temperature*. This model has two important virtues. Phenomenologically, it accounts for the observation that field dependence and temperature dependence are correlated, as noted above. Additionally, effective temperatures are known to be a good description for the effects of high fields in the exponential band-tail hopping model,[28-30] and they also appear in extensions of multiple trapping to include tunneling to the transport edge.[46]

Nonetheless, we do not find that this model gives a satisfactory account for the drift-mobility measurements reported earlier; in effect, our measurements are not consistent with field-dependent dispersion. We shall discuss this issue at length shortly.

The third possibility is that the electric field modifies the escape frequency parameter ν of the multiple-trapping model. Although this model has not been discussed previously, the form $\nu(E) = \nu_0 \exp(-E/E_0)$ gives an adequate agreement with our measurements. We shall return to this model following the next section.

C. Field-dependent dispersion

Perhaps the most intuitive approach that has been proposed for understanding high field effects in amorphous semiconductors is the *effective-temperature* approach.[28,2] Drift mobilities decline sharply with temperature in most amorphous semiconductors, and they rise sharply at high fields. Perhaps the effects of the field can be understood simply by saying that the field raises the effective temperature T_{eff}, which describes the mobility. More specifically, we predict that the features of a low-temperature, nonlinear mobility measured at high fields should be the same as those estimated using a linear model at some higher temperature.

The effective-temperature approach is also known to characterize very well the effects of high fields in the model, which describes transport as due to hopping between localized, band-tail states. This was first proposed by Shklovskii *et al.*[28] The proposal has been confirmed in numerical simulations of dc hopping transport of carriers by Marianer and Shklovskii;[29] they found that the effective temperature $T_{\text{eff}}(E,T)$ was

$$T_{\text{eff}}(E,T) = \sqrt{T^2 + (0.67eaE/k_B)^2}, \qquad (10)$$

where a is a localization length characterizing the band-tail states. Shklovskii also proposed that this effective temperature should characterize transient photocurrents in the hopping model; this proposal was confirmed in "typical rate" calculations by Devlen *et al.*[30]

We have tested this particular effective-temperature form in Fig. 12. In Fig. 12(a), we have plotted the transient drift mobility $\mu = i(t)d^2/Q_0V$ as a function of temperature from several sources. The solid line is a fitting to the temperature dependence of the low-field mobility, as do most of the measured points. The solid circles indicate measurements with fields up to 3.0×10^5 V/cm, which deviate substantially from the low-field limit. The open diamonds represent optically detected time-of-flight measurements at 3×10^5 V/cm; only at the highest temperature do these measurements converge with the low-field form.

In Fig. 12(b), we have replotted all of these measurements using the effective temperature of Eq. (10). We chose the localization radius $a = 5.5$ Å to fit the data. This procedure aligns the high-field measurements with the low field curve very well.
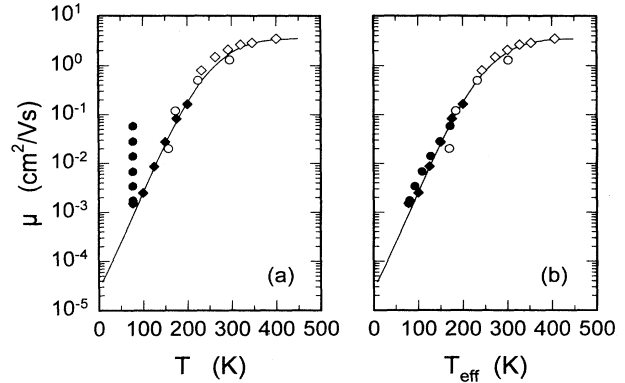
Figure 12 establishes that the effective-temperature

FIG. 12. (a) Transient drift mobility μ measurements as a function of temperature from several sources. The solid line is the low-field multiple-trapping fit for low electric fields. All the data points represent low-field results, excepting the vertical series of solid circles at 77 K. (b) Transient drift mobility is plotted as a function of effective temperature T_{eff}; the effective temperature rationalizes these data, but fails to account for the dispersion properties of the mobility. In this figure, the solid symbols indicate the present work: ◆, 30 kV/cm; ●, fields from 30 to 300 kV/cm. Open symbols indicate published measurements: ○, 170 kV/cm (Ref. 17); ◇, 150 kV/cm. (Ref. 18).

approach accounts for the field dependence of mobilities measured at a particular delay time. The next test of the effective-temperature model is that it should describe the time dependence of the transient measurements as well. We used the following procedure.

In Fig. 13, we have plotted (solid symbols) the measured transient $i(t)d^2/Q_0V$ at 77 K and 3×10^5 V/cm. The effective temperature assigned to this temperature
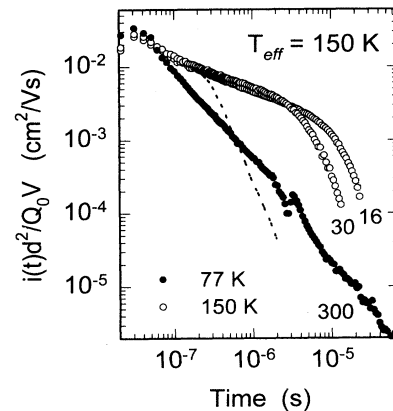

FIG. 13. Application of the effective-temperature approach to predicting the form of the transient photocurrent. The open symbols indicate the mobility function $\mu(t)$ measured at 150 K for the fields shown in kV/cm (cf. Fig. 4). Assuming linear transport, the dashed line indicates the prediction of the effective-temperature model for a field $E = 300$ kV/cm. The solid symbols are the measured transient photocurrent at 77 K and 300 kV/cm, for which the effective-temperature estimate is 150 K. The disagreement is a breakdown of the effective-temperature fitting procedure.

and field is 150 K, so we want to compare this transient with actual measurements at 150 K. Here the procedure is somewhat subtle. Measurements at 150 K and low fields (shown as open symbols) provide a complete description of *linear* electron transport for effective temperatures of 150 K. The transient corresponding to 3×10^5 V/cm and an effective temperature of 150 K is calculated using the 150-K data at low fields and assuming that linear transport extends to 3×10^5 V/cm. We have shown this linear transport extrapolation as the dashed line in the figure.

In an effective-temperature model the measured and predicted transients should agree as a function of time. The two transients do agree near 30 ns, but this simply reflects our fitting procedure in Fig. 12. At longer times the transients disagree. This disagreement occurs because the dispersion parameter of the 77 K, 3×10^5-V/cm measurements is much smaller than that of direct measurements at 150 K.

D. Field-dependent attempt frequency

We were largely successful in fitting our high-field data phenomenologically by allowing for a field-dependent escape frequency in the multiple-trapping form

$$\nu(E) = \nu_0 \exp(-E/E_0), \tag{11}$$

which yields the high-field generalization to Eq. (6):

$$\mu(t, E) \sim \mu_0 [\nu_0 \exp(-E/E_0) t]^{-(1-T/T_0)}. \tag{12}$$

We first show that this form adequately describes the form of the transient decay at high fields; this was the principal failing of the effective-temperature approach. The smooth curves in Fig. 11 are based on the field-dependent escape frequency model using the fitting parameters shown in Fig. 2. Since our measurements were conducted with nearly uniformly absorbed illumination, we averaged the predicted photocurrents from 50 sheets of charges distributed uniformly across the sample. We consider the agreement to be quite satisfactory. The fitting parameters are given in the figure caption; the field $E_0 = 57$ kV/cm.

The field-dependent escape frequency model is a specific case of a *separable* drift mobility

$$\mu(t, E) = \mu(t)\mathcal{M}(\mathcal{E}). \tag{13}$$

This class of models has the wonderful simplification that it is sufficient to examine the functional form of the field dependence at any particular time. In Fig. 2, we have plotted the field dependence of $\mu(t)$ inferred at 30 ns for several temperatures. The solid lines are the predictions of the field-dependent escape frequency model using the same set of fitting parameters. The model offers a very satisfactory account for the current measurements.

VII. REVIEW OF PREVIOUS RESEARCH

We comment briefly on the differences in the published reports on high-field effects for electrons in a-Si:H regarding the presence or absence of *field-dependent dispersion*. It is important to first place this disagreement into perspective: the actual numerical estimates of the field-dependent drift mobility differ only modestly between the various investigators, and in fact we utilized the work of Nebel, *et al.*[40] to extend our knowledge of field dependence down to 40 K. As is evident both in Figs. 1 and 2, the measurements of these authors, of Antoniadis and Schiff, and of the present work are quite consistent.

In modeling the drift measurements, the extent of the apparent field dependence of the dispersion parameter α plays an extremely important role. This parameter is notoriously difficult to estimate convincingly. Regrettably, the conclusions of the four different groups that have addressed the issue of the field dependence of dispersion differ substantially.

In particular, in the present work we find no evidence for the field-dependent dispersion effect; three previous groups have reported it, although they differ significantly in its details. We believe that these differences probably are derived from the very different photoexcitation conditions in the various experiments. In particular, the use of strongly absorbed illumination is certainly problematic in some cases. This statement may surprise the reader, because it is a convention in time-of-flight studies to use strongly absorbed illumination to create a very well defined initial carrier distribution.

For example, two of the experiments used 337-nm illumination in Schottky barrier structures.[47,22] Both experiments inferred field-dependent dispersion from their measurements. However, since 337-nm illumination generates photocarriers within about 100 Å of the metal/a-Si:H interface, one anticipates that a significant fraction of the photogenerated electrons may be lost at lower fields due to back diffusion across the Schottky barrier. This effect has been documented in Schottky barriers in solar cell studies.[48,49] Since back diffusion is suppressed for higher fields, the effect may provide an explanation for the measurements other than field-dependent dispersion.

The remaining measurements were done on *p-i-n* diodes. Nebel *et al.* used 530-nm illumination and a 40-nm a-Si:H:B p^+ layer;[40] they also inferred field-dependent dispersion from their measurements. The relatively long wavelength would mitigate the back-diffusion problem, since the absorption length at 530 nm in a-Si:H is much longer than at 337. However, we estimate that about half of their illumination was absorbed in the p^+ layer, which would probably have led to the p^+ bleeding effect described previously in this paper. The work of Antoniadis and Schiff[19] used *p-i-n* structures and the same wavelength as that of Nebel *et al.*,[40] but claimed field-independent dispersion. The samples in this study had 20-nm-thick microcrystalline p^+ layers. This material is much more transparent than a-Si:H:B; p^+ absorption and subsequent bleeding should have been negligible.

In summary, the present measurements find no evidence for field-dependent dispersion. The three experiments that have inferred field-dependent dispersion[22,40,47] from their photocurrent transient measurements all used illumination conditions which suggest alternate explanations for the data. The features in the transients that lead to an inference of field-dependent dispersion are fairly subtle, and with this exception all five of the available measurements appear reasonably consistent with each other.

VIII. MICROSCOPIC IMPLICATIONS OF HIGH-FIELD TRANSPORT

We commence by summarizing the phenomenological, multiple-trapping description for the temperature and field dependence of the drift mobility $\mu(t)$ described in a previous section:

$$\mu(t) \sim \mu_0 \left[\nu(E)t\right]^{-[1-\alpha(T)]} , \tag{14}$$

$$\alpha(T) = k_B T / \mathcal{E}_0 , \tag{15}$$

$$\nu(E) = \nu_0 \exp(-E/E_0) . \tag{16}$$

We therefore seek microscopic models departing from the exponential band-tail view, which account for the dependences of the three multiple-trapping parameters in a-Si:H upon temperature and field. (1) The mobility prefactor μ_0 is apparently independent of temperature and of electric field. It is also known to depend little upon germanium alloying, which increases $\mathcal{E}_0$. (2) The dispersion parameter $\alpha(T)$ is proportional to the temperature, and is independent of electric field. (3) The attempt-to-escape frequency $\nu(E)$ declines exponentially with electric field E, and is independent of temperature. The exponential decline is counterintuitive, to say the least, since it leads to an exponential increase in mobility.

The two principal transport mechanisms that have been previously examined are carrier *hopping* between the localized band-tail states and *extended state transport* of carriers occupying states above a *mobility edge*. It is now fairly well established that simple hopping models have effective-temperature behavior for high electric fields.[29,30] The present drift mobility measurements do not support this form.

Esipov[46] studied extensions of multiple trapping that incorporated tunneling from the localized band-tail states to the transport edge. For sufficiently high electric fields $eEa > k_B T$ (where a is the localization length of the band-tail states), the model he studied also has effective-temperature behavior, although the quantitative relationship is different than that reported in the hopping calculation of Marianer and Shklovskii.[29] At somewhat lower fields, Esipov discovered a very interesting regime in the band-edge tunneling model, which was not effective-temperature-like; escape of carriers via tunneling contributed more to transport than carrier motion involving states above the transport edge. This regime was a reasonable explanation for the original measurements of Antoniadis and Schiff,[19] but the range of electric fields over which it applies appears to be too small to account for the present work over a larger range of field.

A. Field-dependent mobility edge

The model that we favor involves electric-field dependence of the states near the mobility edge, which appears to lead naturally to an exponential decline of attempt-frequency $\nu(E) = \nu_0 \exp(-E/E_0)$. First, note that theoretical descriptions of the mobility edge suggest that the *localization length* a of band-tail states diverges as the state energy approaches the mobility edge.[50,51] We therefore expect that these very shallow states should be treated as delocalized in the mobility-edge model; this idea has been suggested fairly frequently in the mobility-edge literature. In particular, the states lying within $\mathcal{E}_C - \mathcal{E} \sim Ea(\mathcal{E})$ of the zero-field edge $\mathcal{E}_C$ lose their barriers to thermal emission of a trapped electron in the direction of the applied field. Of course even deep levels are technically delocalized by an electric field; this affects multiple trapping strongly when the zero-temperature tunneling rate exceeds the thermal emission rate.[46]

The model of a field-dependent mobility edge finds some experimental support in the observations of polarization-dependent electroabsorption effects in a-Si:H. These measurements reveal a noticeable, electric-field induced anisotropy to optical transitions involving states near the valence and conduction band mobility edges.[44,45]

We therefore propose the following hypothesis for the effects of an *electric-field-dependent mobility edge* upon multiple-trapping transport. We assume a linear dependence of the edge's position upon electric field:

$$\mathcal{E}_c(E) = \mathcal{E}_c - b(eE) , \tag{17}$$

where e is the electronic charge and b is a length parameter, which presumably reflects the localization length of states near $\mathcal{E}_c(E)$.

We further assume the detailed balance relation between the attempt-to-escape frequency ν, the capture coefficient b_t governing capture of extended state carriers into localized bandtail states, and the "effective" density of states at the mobility-edge N_c:

$$\nu = N_c b_t . \tag{18}$$

Assuming that b_t does not vary with the field, we have for an exponential band-tail $g(\mathcal{E}) = g_0 \exp(\mathcal{E}/\mathcal{E}_0)$:

$$N_c(E) = N_c \exp(-beE/\mathcal{E}_0) , \tag{19}$$

$$\nu(E) = \nu_0 \exp(-beE/\mathcal{E}_0) . \tag{20}$$

These hypotheses lead to the phenomenological, exponential field dependence of $\nu(E) = \nu_0 \exp(-E/E_0)$. The parameter E_0 estimated experimentally can now be reinterpreted in terms of the parameter b describing mobility-edge states and the band-tail width $\mathcal{E}_0$:

$$E_0 = \mathcal{E}_0 / be . \tag{21}$$

For the principal specimen studied in the present work, we have $E_0 = 57 \times 10^3$ V/cm, $\mathcal{E}_0 = 23$ meV, and hence $b = 40$ Å.

This model predicts that the parameter E_0 should be proportional to the band-tail width (presuming that the length b is invariant). This prediction is consistent with the very limited high-field measurements published for electrons in a-Si$_{1-x}$Ge$_x$:H,[19] which showed an increase in E_0 as $\mathcal{E}_0$ increased.

B. Alternative models

One suspects that the phenomenological result $\nu = \nu_0 \exp(-E/E_0)$ may find other explanations besides a field-dependent mobility edge. Perhaps the first model that comes to mind when considering high-field effects is simple field ionization of a trap, of which the Poole-Frenkel model is the best known example. The field-dependent mobility-edge model just described may actually be the generalization of Poole-Frenkel type models to the case where ionization involves a mobility edge: The field lowers the barrier for reemission by lowering the threshold for ionization to extended states in both cases.

A fairly compelling argument has been given recently by Yelon and Movaghar,[52] and Yellon, Movaghar, and Branz[53,54] that the "Meyer-Neldel" behavior commonly observed in noncrystalline materials is a consequence of an increase in attempt-frequencies ν with increasing trap energy. Such an increase is predicted when electron trapping and emission typically involve several phonons. Although multiple-trapping models normally invoke an energy independent value for ν, the measurements do not exclude energy dependence. Peled, Schein and Glatz[32] and Schein[3] proposed that the electric-field dependence of the (nondispersive) drift mobilities in molecularly doped polymers reflects the Meyer-Neldel behavior: as an electric field lowers the activation barrier for transport, there is a compensating lowering of the attempt-to-hop frequency. Further study of this approach for a dispersive transport system would obviously be of interest.

Finally, Overhof[13,14] demonstrated that multiple-trapping behavior can emerge from the effects of long-range potential fluctuations on a transport band. Applying this model to drift-mobility measurements in undoped a-Si:H, Overhof[14] calculated that the corresponding nonlinear behavior should be observed only for very low fields $E < 10^3$ V/cm. The calculation would thus tend to exclude potential fluctuations as the origin for the high-field effects for electrons in a-Si:H reported here and in previous work, as has previously been inferred by Liu et al.[55]

Note added in proof. Two papers on effective-temperature models have been published recently. Palsule et al. measured photoconductivity in the field range 10^4–10^5 V/cm.[56] Muschik and Schwarz studied the field dependence of low-temperature recombination in a-Si:H.[57] Both groups claimed the validity of the effective-temperature approach but disagreed on the functional dependence on the actual temperature. Their proposed forms are also significantly different from that of Mariamer and Shklovskii.[29]

ACKNOWLEDGMENTS

[1] C. Canali, F. Nava, and L. Reggiani, in *Hot-Electron Transport in Semiconductors*, edited by L. Reggiani, Topics in Applied Physics Vol. 58 (Springer, Berlin, 1985), p. 87.

[2] B. Movaghar, A. Yelon, and M. Meunier, Chem. Phys. **146**, 389 (1990).

[3] L. B. Schein, Philos. Mag. B **65**, 795 (1992).

[4] H. Bäßler, Phys. Status Solidi B **175**, 15 (1993).

[5] T. Tiedje, J. M. Cebulka, D. L. Morel, and B. Abeles, Phys. Rev. Lett. **46**, 1425 (1981).

[6] J. Orenstein and M. Kastner, Phys. Rev. Lett. **46**, 1421 (1981).

[7] J. M. Hvam and M. H. Brodsky, Phys. Rev. Lett. **46**, 371 (1981).

[8] N. F. Mott, Adv. Phys. **16**, 49 (1967).

[9] M. Silver, G. Schönherr, and H. Bäßler, Phys. Rev. Lett. **48**, 352 (1982).

[10] M. Grünewald and P. Thomas, Phys. Status Solidi B **94**, 125 (1979).

[11] M. Grünewald, B. Movaghar, B. Pohlmann, and D. Würtz, Phys. Rev. B **32**, 8191 (1985).

[12] D. Monroe, Phys. Rev. Lett. **54**, 146 (1985).

[13] H. Overhof, J. Non-Cryst. Solids **59&60**, 57 (1983).

[14] H. Overhof, in *Amorphous Silicon Technology—1992*, edited by M. J. Thompson et al., MRS Symposia Proceedings No. 258 (Materials Research Society, Pittsburgh, 1992), pp. 681–692.

[15] E. A. Schiff, R. I. Devlen, H. T. Grahn, and J. Tauc, Appl. Phys. Lett. **54**, 1911 (1989).

[16] R. I. Devlen, E. A. Schiff, and J. Tauc, in *Amorphous Silicon Technology—1989*, edited by A. Madan et al., MRS Symposia Proceedings No. 149 (Materials Research Society, Pittsburgh, 1989), pp. 107–111.

[17] R. I. Devlen, J. Tauc, and E. A. Schiff, J. Non-Cryst. Solids **114**, 567 (1989).

[18] G. Juška, J. Kočka, K. Arlauskas, and G. Jukonis, Solid State Commun. **75**, 531 (1990).

[19] H. Antoniadis and E. A. Schiff, Phys. Rev. B **43**, 13 957 (1991).

[20] S. Imao et al., Jpn. J. Appl. Phys. **7B**, L1227 (1991).

[21] J. Kočka et al., Phys. Rev. B **45**, 6593 (1992).

[22] K. Murayama, H. Oheda, S. Yamasaki, and A. Matsuda, Solid State Commun. **81**, 887 (1992).

[23] C. E. Nebel and R. A. Street, Int. J. Mod. Phys. B **17**, 1207 (1993).

[24] Q. Gu, E. A. Schiff, J. Chévrier, and B. Equer, in *Amorphous Silicon Technology—1993*, edited by E. A. Schiff et al., MRS Symposia Proceedings No. 297 (Materials Research Society, Pittsburgh, 1993) p. 425.

[25] C. E. Nebel and R. A. Street, in *Amorphous Silicon Technology—1994*, edited by E. A. Schiff et al., MRS Sym-

posia Proceedings No. 336 (Materials Research Society, Pittsburgh, 1994), pp. 383–388.

[26] H. Scher and E. Montroll, Phys. Rev. B **12**, 2455 (1975).

[27] H. Scher, M. F. Shlesinger, and J. T. Bendler, Phys. Today **44** (1), 26 (1991).

[28] B. I. Shklovskii, E. I. Levin, H. Fritzsche, and S. D. Baranovskii, in *Transport, Correlations and Structural Defects*, edited by H. Fritzsche (World Scientific, Singapore, 1990), p. 161.

[29] S. Marianer and B. I. Shklovskii, Phys. Rev. B **46**, 13 100 (1992).

[30] R. I. Devlen, H. Antoniadis, E. A. Schiff, and J. Tauc, Philos. Mag. B **68**, 341 (1993).

[31] V. I. Arkhipov and H. Bäßler, Philos. Mag. Lett. **69**, 241 (1994).

[32] A. Peled, L. B. Schein, and D. Glatz, Phys. Rev. B **41**, 10 835 (1990).

[33] B. Equer and J. B. Chévrier, in *Amorphous Silicon Technology—1992* (Ref. 14), pp. 1045–1056.

[34] J. Chévrier, Ph.D. thesis, Université de Paris VII, 1993.

[35] L. Yang, L. Chen, S. Wiedeman, and A. Catalano, in *Microcrystalline Semiconductors: Materials Science and Devices Materials Research Society Symposium Proceedings*, edited by P. M. Fauchet *et al.*, MRS Symposia Proceedings Vol. 283 (Materials Research Society, Pittsburgh, 1993), pp. 463–470.

[36] R. M. A. Dawson, S. Nag, C. R. Wronski, and M. Maley, in *The Conference Record of the Twenty-Third IEEE Photovoltaic Specialists Conference—1992* (IEEE, Piscataway, NJ, 1992), pp. 960–965.

[37] R. A. Street, J. Zesch, and M. J. Thompson, Appl. Phys. Lett. **43**, 672 (1983).

[38] H. Antoniadis and E. A. Schiff, Phys. Rev. B **44**, 3627 (1991).

[39] M. Vaněček, J. Kočka, E. Šipek, and A. Třiska, J. Non-Cryst. Solids **114**, 447 (1989).

[40] C. E. Nebel, R. A. Street, N. M. Johnson, and J. Kočka, Phys. Rev. B **46**, 6789 (1992).

[41] Q. Wang, H. Antoniadis, E. A. Schiff, and S. Guha, Phys. Rev. B **47**, 9435 (1993).

[42] T. Tiedje, in *Hydrogenated Amorphous Silicon II*, edited by J. D. Joannopoulos and G. Lucovsky (Springer-Verlag, New York, 1984), pp. 261–300.

[43] P. N. Butcher and J. D. Clark, Philos. Mag. B **42**, 191 (1980).

[44] G. Weiser, U. Dersch, and P. Thomas, Philos. Mag. B **57**, 721 (1988).

[45] Y. Tsutsumi *et al.*, J. Non-Cryst. Solids **164–166**, 893 (1993).

[46] S. E. Esipov, Phys. Rev. B **44**, 7930 (1991).

[47] J. Ichi Nakata, S. Nakajima, S. Imao, and Y. Inuishi, Jpn. J. Appl. Phys. **33**, 5640 (1994).

[48] D. Gutkowicz-Krusin, C. R. Wronski, and T. Tiedje, Appl. Phys. Lett. **38**, 87 (1981).

[49] P. J. McElheny, P. Chatterjie, and S. J. Fonash, J. Appl. Phys. **69**, 7674 (1991).

[50] N. F. Mott, *Conduction in Non-Crystalline Solids* (Oxford, University Press Oxford, 1987).

[51] E. N. Economou, C. M. Soukoulis, M. H. Cohen, and S. John, in *Disordered Semiconductors*, edited by M. A. Kastner, G. A. Thomas, and S. R. Ovshinsky (Plenum, New York, 1987), pp. 681–704.

[52] A. Yelon and B. Movaghar, Phys. Rev. Lett. **65**, 618 (1990).

[53] A. Yelon, B. Movaghar, and H. M. Branz, Phys. Rev. B **46**, 12 244 (1992).

[54] H. M. Branz, A. Yelon, and B. Movaghar, in *Amorphous Silicon Technology—1994* (Ref. 25), pp. 159–164.

[55] E. Z. Liu *et al.*, Philos. Mag. B **70**, 109 (1994).

[56] C. Palsule, S. Yi, and S. Gangopadhyay, Phys. Rev. Lett. **73**, 3145 (1994).

[57] T. Muschik and R. Schwarz, Phys. Rev. B **51**, 5078 (1995).